IJCRT.ORG

ISSN: 2320-2882



INTERNATIONAL JOURNAL OF CREATIVE RESEARCH THOUGHTS (IJCRT)

An International Open Access, Peer-reviewed, Refereed Journal

High Precision Precipitation System Analysis For Improved Weather Reliability

Chandra Sekhar.K¹, G.Manjusha², K.Gowthami³, D.Jyothika⁴, M.Dhanush Sai⁵

¹Assistant Professor, Department of ECE, Raghu Engineering College, Dakamarri, Vizag, AP, India.

^{2,3,4,5} Students, Department of ECE, Raghu Institute of Technology, Dakamarri, Vizag, AP, India.

Abstract

Weather Radar has been a crucial tool for monitoring precipitation intensity and extent for many years. The National Weather Service's Nexrad radar system exemplifies this technology, providing quantitative measurements of precipitation, wind speed and direction, and other meteorological data. Additionally, Terminal Doppler Weather Radar (TDWR) systems are used near airports to detect dangerous micro bursts, which are strong downdrafts that pose hazards to aircraft during take-off and landing. These advancements have significantly enhanced weather forecasting and safety measures.

Key words: Weather Radar, Doppler, TDWR

I. Introduction

Most modern weather radars utilise a pulse-Doppler technique that, in addition to providing estimates of precipitation rate, also enable the detection of droplet motion with respect to the radar and, as a result, can be used to determine radial wind speeds [1][2]. Weather radars usually work with three main types of data. In the reflectivity mode, return echoes from targets are analyzed for their intensities to establish the precipitation rate in the scanned volume. In the Doppler mode, the precipitation's motion is calculated[8][11]. Finally, in the polarization operational mode, orthogonal polarization pulses are used to evaluate drop shapes and distinguish amongst different precipitation types, such as rain, snow, or hail [7].

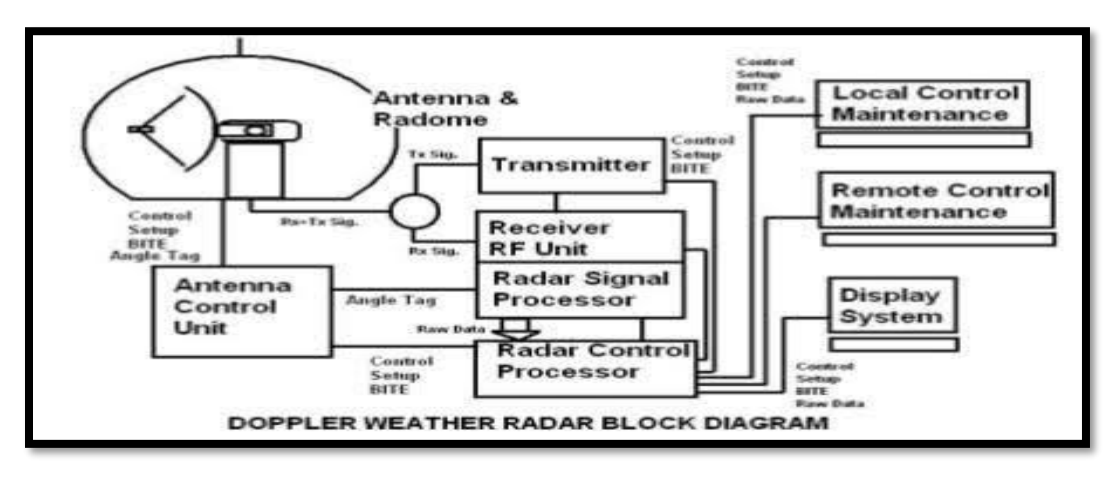


Figure 1: Block Diagram of Weather Radar

The block diagram illustrates the key components of a Doppler Weather Radar system, showcasing the flow of data and control signals through various units[3][4]. The **Antenna & Radome** unit, located at the top left, is responsible for transmitting radar signals and receiving echoes reflected from atmospheric particles, which are then analyzed to detect precipitation and measure velocity[5][6]. The antenna is protected by a radome and is controlled by the **Antenna Control Unit** that manages its orientation and movement, allowing it to cover a wide area. The antenna control also provides "Angle Tag" data, indicating the direction of radar scans[9][10][13].

II. Algorithms for Weather Radar Systems

The Algorithms that are widely used for Weather Radar Systems are tabulated below.

Table 1: Algorithms for Weather Radar

Algorithm	Purpose			
Vertically Integrated	Estimates the total mass of precipitation in a cloud, helping assess			
Liquid (VIL)	storm intensity.			
VIL Density	Calculates precipitation concentration by dividing VIL by cloud			
	height, providing clues about the likelihood of large hail[15][16].			
Potential Wind Gust	Estimates wind speeds beneath a storm cell using VIL and cloud			
	echo tops, aiding in severe weather warnings.			
Hail Algorithms	Detects the presence of hail and estimates its probable size based on			
	radar reflectivity, improving storm impact forecasts.			
Meso-cyclone	Identifies rotating storm systems by analyzing velocity changes in a			
Detection	circular pattern, which may indicate tornado development.			
Tornado Vortex	Detects strong rotational velocity thresholds over multiple scanning			
Signature (TVS)	angles, indicating possible tornado formation.			
Wind Shear in Low	Identifies rapid changes in wind speed/direction to detect			
Levels	downdrafts, downbursts, micro bursts, and gust fronts.			
Echo Top Algorithm	Determines the highest altitude at which significant precipitation is			
	detected, useful for assessing storm strength[12][14].			

	Lightning Detection	Identifies areas of high lightning activity using radar and sat		
	Algorithm data, enhancing severe weather warnings.			
Turbulence Detection Analyzes rapid wind speed fluctuations to d		Analyzes rapid wind speed fluctuations to detect turbulence zones,		
	Algorithm	crucial for aviation safety.		

III. Results & Discussions

a) SNR vs Range

The graph depicts the relationship between Signal-to-Noise Ratio in dB and Target Range in km for a weather radar system. The solid blue line represents how SNR decreases as the target range increases, indicating that detection capability weakens with distance. Two dashed lines represent "Objective Detectability" and "Threshold Detectability," marking the minimum SNR levels required for reliable and marginal detection, respectively. The background is color-coded, indicating the green region as the sufficient SNR for detection and the red region as the area of unreliable detection. A vertical black dashed line indicates the "Max Range," which is the area beyond which the targets are not effectively detected.

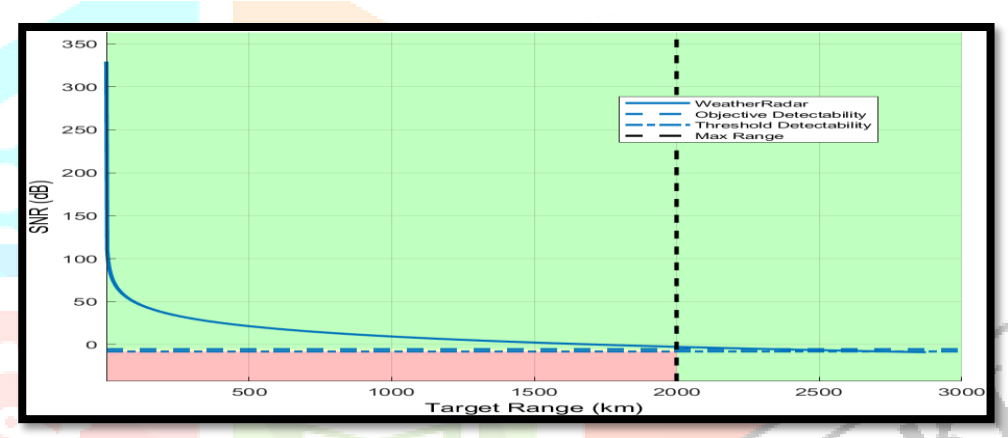


Figure 2: Simulation Result for SNR vs Range

b) CNR vs Range

The graph showins the Carrier-to-Noise Ratio (CNR) in decibels as a function of target range (km). Several curves are present, each showing different detection thresholds and conditions: "Weather Radar," "Objective Detectability," "Threshold Detectability," and "Horizon Range." The plotted lines are near the zero dB level, indicating that the CNR is very low across the target range. It implies that the ability of the radar system to detect targets has decreased substantially at a large range, which might be due to signal attenuation or propagation loss.

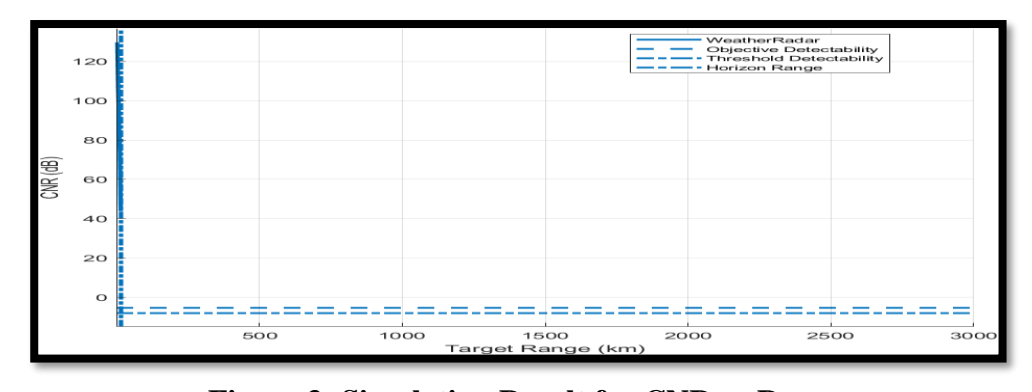


Figure 3: Simulation Result for CNR vs Range

c) Link Budget

The graph is about the presentation of the required Signal-to-Noise Ratio in decibels for a weather radar system. The chart has bar segments, where red-coloured bars show positive SNR values that indicate high requirements, and the green-colored bar indicates a negative SNR value, that means reduction in the SNR requirement. The dotted blue line refers to a baseline level at around -5.30 dB. The values that appear within the bars (10.76 dB, -18.06 dB, and 2.00 dB) correspond to the respective contributions of conditions to the required SNR in the system. The fact that both positive and negative values occur means that certain conditions add to the required SNR while others subtract from it, thus making targets detectable in the radar system.

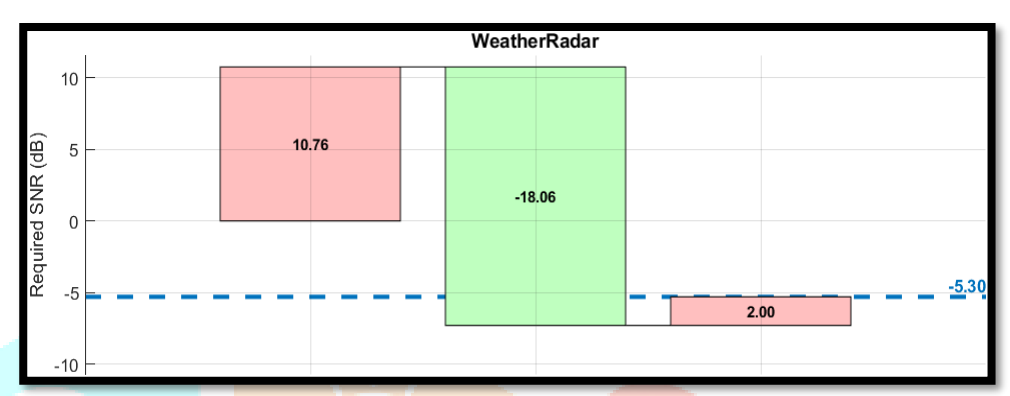


Figure 4: Simulation Result for Link Budget

d) Environmental Losses

The graph is shown of the different propagation and loss factors which influence the performance of weather radar as a function of target range in km. It has four subplots: Radar Propagation Factor, Precipitation Loss, Lens Effect Loss, and Atmospheric Gas Loss. The Radar Propagation Factor is nearly constant around 1 dB for all target ranges; therefore, it indicates that the signal propagation characteristics are not changed much. Precipitation Loss, Lens Effect Loss, Atmospheric Gas Loss is almost 0 dB in value, implying that their effect is negligible over this range.

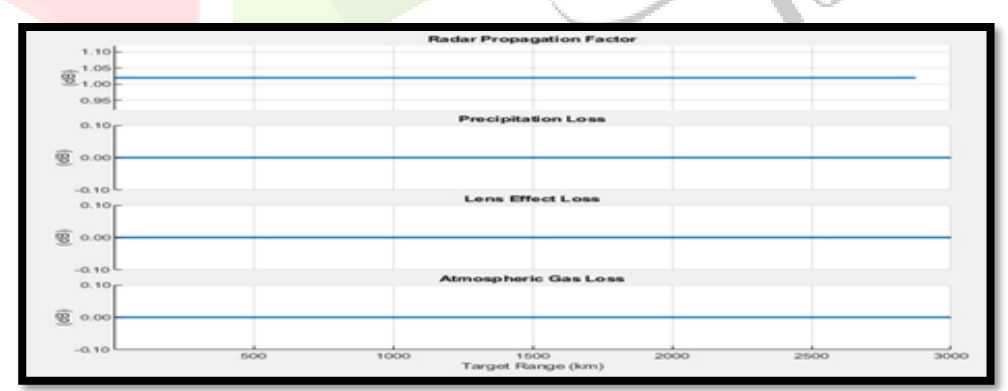


Figure 5: Simulation Result for Different Environmental Losses

e) Pd vs Range

The graph represents the Probability of Detection (Pd) as a function of Target Range (km) for a weather radar system. The blue curve shows the radar's detection probability, while the dashed lines indicate key reference points: Objective Pd (higher probability threshold), Threshold Pd (minimum required probability for reliable detection), and Max Range (marked by a vertical dashed black line). The graph shows that at short ranges, the radar maintains nearly perfect detection capability. However, as the target range approaches 2000 km (the max range limit), the probability of detection starts to drop. Beyond 2500 km, the

detection probability decreases rapidly, nearing zero around 3000 km. This suggests that while the radar performs well within its operational range, detection becomes increasingly unreliable at long distances due to factors like signal attenuation, environmental conditions, and system limitations.

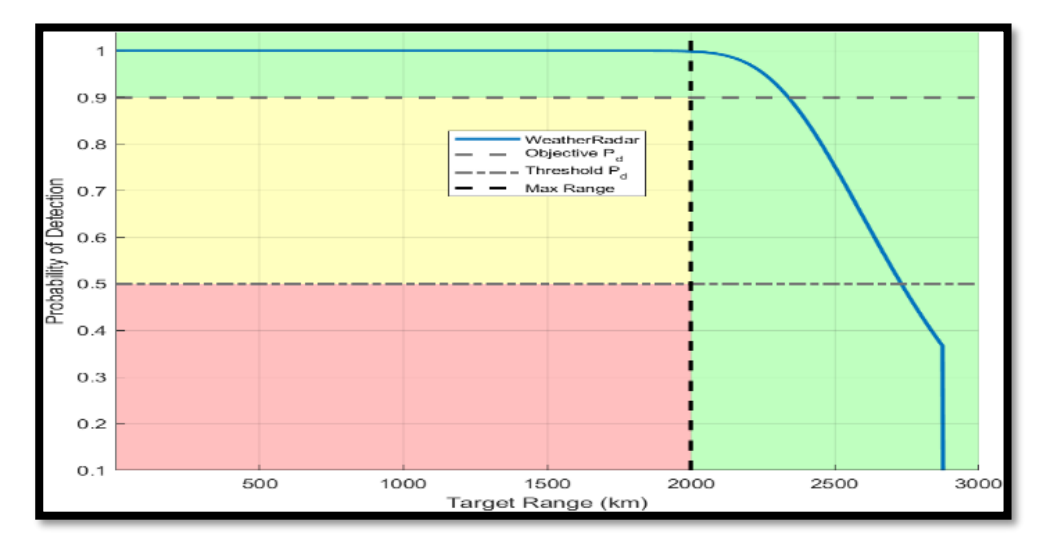


Figure 6: Simulation Result for Probability of Detection vs Range

f) Pd vs SNR

The graph illustrates the Probability of Detection (Pd) as a function of Signal-to-Noise Ratio (SNR in dB) for a weather radar system, with a false alarm probability (P_{fa}) of 0.001. The blue curve represents how detection probability increases with higher SNR values. The dashed lines indicate the Objective Pd (higher detection probability requirement) and Threshold Pd (minimum acceptable detection probability). The graph shows that at lower SNR values (below -8 dB), detection probability remains low. As SNR improves, the probability of detection increases steeply, surpassing the threshold and objective detection probabilities. The contour lines indicate different false alarm rates, showing the system's sensitivity under various conditions.

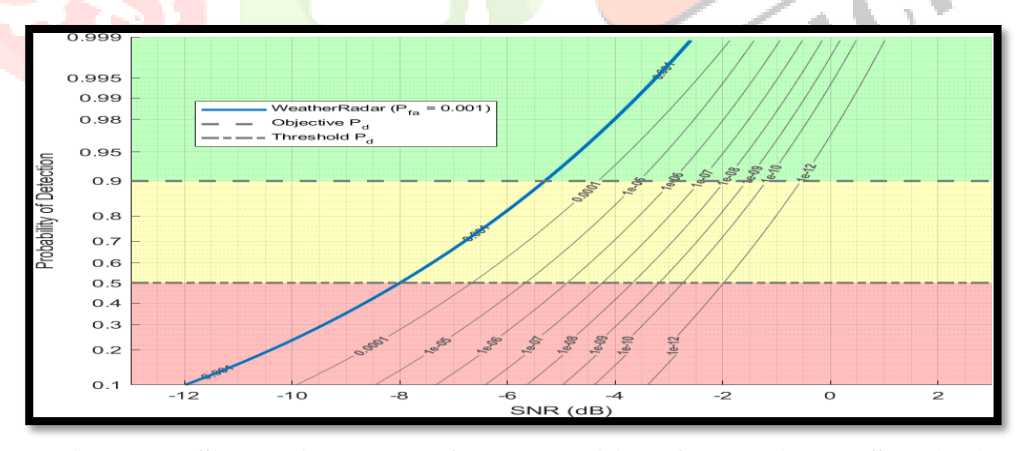


Figure 7 : Simulation Result for Probability of Detection vs SNR(dB)

g) Range-Doppler Coverage

This graph illustrates the relation between Unambiguous Range (km) and First Blind Speed (m/s) for a weather radar with an operating frequency of 2.8 GHz. The inverse nature of these parameters is well shown in the curve in the form of blue; it can be inferred that with the increase in the unambiguous range, the first blind speed decreases. Both the axes are on logarithmic scales and have depicted an exponential relationship between these parameters. A particular point is indicated on the graph, which gives values

for: Unambiguous Range (*Ru*): 468.426 km; First Blind Speed (*vb*): 17.131 m/s Pulse Repetition Frequency (PRF): 0.32 kHz

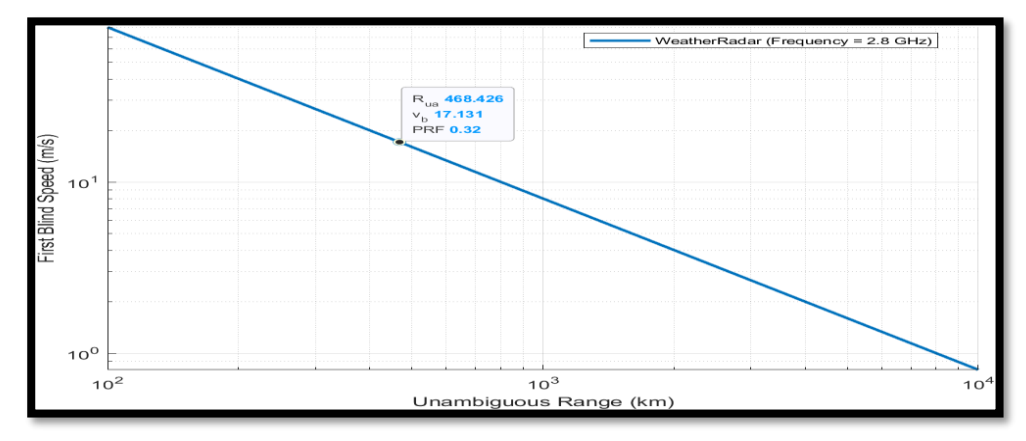


Figure 8 : Simulation Result for Range Doppler Coverage

h) Metrics and Requriments

The following table provides a comparative analysis of the Radar performance metrics categorized under Threshold, Objectives, and Weather Radar values. Each row contains a key radar parameter along with its unit of measurement. The Threshold column shows the minimum acceptable performance, and the Objectives column defines the target desired values for optimum performance. The column for Weather Radar depicts the actual performance the system has achieved.

Table 2 : Comparison of Radar Performance Metrics

Metrics	Threshold	Objectives	Weather Radar
Probability of Detection	0.5	0.9	0.9989
Min Detectable Signal	-90 dBm	-120 dBm	-120.4 dBm
Min Range	3000 M	150 M	224.8 M
Unambiguous Range	100 Km	115 Km	468.4 Km
Range Resolution	400 M	350 M	299.8 M
First Blind Speed	10 m/s	15 m/s	17.13 m/s
Range Rate Resolution	5 m/s	1 m/s	0.2677 m/s
Probability of True Track	0.9	0.95	1
Probability of False Track	1e-06	1e-08	7.459e-12
Effective isotropic Radiated	1.3e+04 MW	1.5e+04 MW	1.581e+04 MW
Power			

IV. Conclusion

Weather radar observations have a lot of potential for many uses, especially in the hydrological field. This is readily disclosed for emergency management, the evaluation of damage from extreme occurrences, and the delivery of a number of prediction services. This Work proposes an overview of different Performance Metrics Range, Resolution, Probability of Detection, Probability of True Track etc of Weather Radar. All the Simulations are carried out using Matlab Tool and the Results are compared with the Standard Performance Metrics.

V. References

- 1. Bonci, L.; Malcevschi, S.; Belvisi, M.; Piccini, C.; D'Ambrogi, S.; Ercole, S.; Giovagnoli, M.C.; Franchi, G.; Morelli, E.; Parente, S. Dynamic Glossary for the Environment and Landscape; Manuals and Guidelines 78/2012; ISPRA: Rome, Italy, 2012.
- 2. Mahoney, J.R. AMS 2000: A Strategic Review. Bull. Am. Meteorol. Soc. **1990**, 71, 504–506.
- 3. Mapes, J.A.; Johnson, R.H.; Mapes, B.E. Mesoscale Processes and Severe Convective Weather. In Severe Convective Storms; American Meteorological Society: Boston, MA, USA, 2001; pp. 71–122.
- 4. Economic Losses from Climate-Related Extremes in Europe. Available online: https://www.eea.europa.eu/ims/economic-losses-from-climate-related (accessed on 19 December 2021).
- 5. Bringi, V.; Zrnic, D. Polarization Weather Radar Development from 1970–1995: Personal Reflections. Atmosphere **2019**, 10, 714.
- 6. Battan, L.J. Radar Observation of the Atmosphere; University of Chicago Press: Chigago, IL, USA, 1981.
- 7. File: Weather-Radar-Blind-Zone.png—Wikimedia Commons. Available online: https://commons.wikimedia.org/wiki/File:Weather-radar-blind-zone.png (accessed on 8 January 2022).
- 8. Sokol, Z.; Szturc, J.; Orellana-Alvear, J.; Popová, J.; Jurczyk, A.; Célleri, R. The Role of Weather Radar in Rainfall Estimation and Its Application in Meteorological and Hydrological Modelling—A Review. Remote Sens. 2021, 13, 351.
- 9. Rahimi, A.R.; Holt, A.R.; Upton, G.J.G.; Krämer, S.; Redder, A.; Verworn, H.R. Attenuation Calibration of an X-Band Weather Radar Using a Microwave Link. J. Atmos. Ocean. Technol. 2006, 23, 395–405.
- 10. Bringi, V.N.; Chandrasekar, V. Polarimetric Doppler Weather Radar: Principles and Applications; Cambridge University Press: Cambridge, UK, 2001; p. 636.
- 11. R. M. Rauber and S. W. Nesbitt, "Precipitation estimation with radar," in Radar Meteorology. Hoboken, NJ, USA: Wiley, 2018, pp. 310–338.
- 12. S. Sebastianelli, F. Russo, F. Napolitano, and L. Baldini, "On precipitation measurements collected by a weather radar and a rain gauge network," Natural Hazards Earth Syst. Sci., vol. 13, no. 3, pp. 605–623, Mar. 2013.
- 13. He G, Li G, Zou X, et al. A Velocity Dealiasing Scheme for Synthetic C-Band Data from China's New Generation Weather Radar System (CINRAD)[J]. Journal of Atmospheric and Oceanic Technology, 2012, 29(9):1263-1274.
- 14. L. Cuo, T. C. Pagano, and Q. J. Wang, "A review of quantitative precipitation forecasts and their use in short-to medium-range streamflow forecasting," J. Hydrometeorol., vol. 12, pp. 713–728, Oct. 2011.

- 15. Seed, A., E. Duthie, and S. Chumchean. Rainfields: The Australian Bureau of Meteorology system for quantitative precipitation estimation. Preprints, 33rd AMS Conf. Radar Meteorology (Cairns, Australia). Vol. 6. No. 10. 2007.
- 16. M. N. Anagnostou et al., "Advancing precipitation estimation and streamflow simulations in complex terrain with X-band dual polarization radar observations," Remote Sens., vol. 10, no. 8, p. 1258, Aug. 2018. [11].

